Identification of a protein–protein interaction between KCNE1 and the activation gate machinery of KCNQ1

Anatoli Lvov, Steven D. Gage, Virla M. Berrios, and William R. Kobertz

Department of Biochemistry and Molecular Pharmacology, Programs in Neuroscience and Chemical Biology, University of Massachusetts Medical School, Worcester, MA 01605

KCNQ1 channels assemble with KCNE1 transmembrane (TM) peptides to form voltage-gated K⁺ channel complexes with slow activation gate opening. The cytoplasmic C-terminal domain that abuts the KCNE1 TM segment has been implicated in regulating KCNQ1 gating, yet its interaction with KCNQ1 has not been described. Here, we identified a protein–protein interaction between the KCNE1 C-terminal domain and the KCNQ1 S6 activation gate and S4–S5 linker. Using cysteine cross-linking, we biochemically screened over 300 cysteine pairs in the KCNQ1–KCNE1 complex and identified three residues in KCNQ1 (H363C, P369C, and I257C) that formed disulfide bonds with cysteine residues in the KCNE1 C-terminal domain. Statistical analysis of cross-link efficiency showed that H363C preferentially reacted with KCNE1 residues H73C, S74C, and D76C, whereas P369C showed preference for only D76C. Electrophysiological investigation of the mutant K⁺ channel complexes revealed that the KCNQ1 residue, H363C, formed cross-links not only with KCNE1 subunits, but also with neighboring KCNQ1 subunits in the complex. Cross-link formation involving the H363C residue was state dependent, primarily occurring when the KCNQ1–KCNE1 complex was closed. Based on these biochemical and electrophysiological data, we generated a closed-state model of the KCNQ1–KCNE1 cytoplasmic region where these protein–protein interactions are poised to slow activation gate opening.

INTRODUCTION

KCNQ1 (Q1 or Kv7.1) voltage-gated K⁺ channels are composed of archetypical six transmembrane (TM) subunits that tetramerize to form an ion-conducting pore domain (S5–S6) surrounded by four voltage-sensing domains (S1–S4). The cytoplasmic S4–S5 linker between these two functionally distinct domains mechanically couples voltage sensing to activation gate opening and closing. Although homotetrameric Q1 channels generate a fast activating delayed rectifier K⁺ current when expressed in standard expression systems (Barhanin et al., 1996; Sanguinetti et al., 1996), in native tissues the channel is obligatorily coassembled with one of the five members of the KCNE family of regulatory subunits (KCNE1-5; encoded proteins are MinK and MiRP1-4, respectively) (McCrossan and Abbott, 2004). Coassembly with these type I TM peptides markedly changes the voltage gating of the Q1 channel, allowing it to properly function in different tissues, including cardiac myocytes, cochlea, renal, gastrointestinal, and pulmonary epithelia (Barhanin et al., 1996; Sanguinetti et al., 1996; Mall et al., 2000; Schroeder et al., 2000; Nicolas et al., 2001; Roepke et al., 2006). Modulation of Q1 channel function by all five KCNE proteins has been observed; however, Q1's association with KCNE1 (E1) has been studied more thoroughly due to the involvement of this complex in several pathophysiological conditions ranging from inherited ventricular arrhythmias (Splawski et al., 1997b) to deafness (Vetter et al., 1996; Tyson et al., 2000). In cardiomyocytes, the Q1–E1 complex conducts the slowly activating and deactivating, yet apparently non-inactivating, I$_{Ks}$ current (Sanguinetti and Jurkiewicz, 1990; Barhanin et al., 1996; Sanguinetti et al., 1996), which is involved in the repolarization phase of cardiac action potential. Mutations in either Q1 (Chouabe et al., 1997; Napolitano et al., 2005) or E1 (Splawski et al., 1997b, 2000) that decrease the conductance of the complex prolong the cardiac action potential and cause arrhythmias, including long QT syndrome. In the inner ear, where Q1–E1 complex provides a passage for K⁺ to the endolymph in the cavities of the cochlear labyrinth, these detrimental mutations can cause congenital deafness (Chouabe et al., 1997; Neyroud et al., 1997; Splawski et al., 1997a).

In contrast to K⁺ channel interactions with strictly cytoplasmic modulators, such as G proteins, KChIPs, or Kvβ subunits, the site of action of E1, a single-pass membrane protein, has been sought in the extracellular, cytoplasmic, and membrane-embedded regions of Q1.

The Rockefeller University Press $30.00
J. Gen. Physiol. Vol. 135 No. 6   607–618
www.jgp.org/cgi/doi/10.1085/jgp.200910386

607

Initial electrophysiological studies focused on the membrane-embedded portion of the Q1–E1 complex, and it was proposed that the E1 TM segment lined the conductivity pathway (Wang et al., 1996; Tai and Goldstein, 1998) of the complex. However, the many high resolution structures of the tightly packed helices of the K⁺ channel pore domain have made this location infeasible. More recent electrophysiological investigations have relocated the E1 TM on the backside of the Q1 pore domain (Tapper and George, 2001; Melman et al., 2004; Panaghie et al., 2006). The discovery of atrial fibrillation mutations in the extracellular S1–S2 loop of Q1 (Y.H. Chen et al., 2003; Hong et al., 2005; Lundby et al., 2007) has shifted attention toward the extracellular domains of the Q1–E1 complex. Two different studies using cysteine cross-linking have identified protein–protein interactions between the E1 N terminus and the extracellular tops of the S1 and S4 segments, and the pore domain of Q1 (Xu et al., 2008; Chung et al., 2009). In total, these studies position the E1 TM segment in a cleft between the pore and voltage-sensing domains of the Q1 channel. A recent coimmunoprecipitation study of the cytoplasmic parts of the Q1–E1 complex has identified a large stretch of residues at the E1 C terminus that binds to the subunit identification ("tetramerization") domain of the Q1 channel, providing an anchoring point at the C terminus (Haitin et al., 2009).

A cytoplasmic domain of E1 that has been of continual interest comprises the ∼20 residues that abut the membrane, which are seemingly ideally located near the cytoplasmic machinery of Q1 responsible for voltage-dependent gating. One of the first mutagenesis investigations of E1 (then I_{Ks}) showed that point mutations in this C-terminal domain greatly affect channel activity (Takumi et al., 1991). Subsequent deletion and chimera studies have indicated that this domain is critical for the characteristic slow activation kinetics of the Q1–E1 complex (Tapper and George, 2000; Gage and Kobertz, 2004). Moreover, several missense point mutants that cause long QT syndrome cluster to this C-terminal domain in E1 (Splawski et al., 2000; Schulze-Bahr et al., 2001; Ma et al., 2003; Lai et al., 2005; Napolitano et al., 2005). Periodicity analysis of mutagenic perturbation experiments have shown that this membrane-abutting domain of E1 adopts an α-helical structure when split in half at a conserved proline residue (Rocheleau et al., 2006). This secondary structure predicts that all of the known long QT mutations in this domain will face the Q1 channel. Despite the extensive study by several laboratories, the protein–protein interactions between the E1 C-terminal domain and Q1 have remained uninvestigated.

To identify the Q1 cytoplasmic surfaces that interact with the E1 C-terminal domain, we used oxidant-mediated disulfide bond formation between exogenous cysteine point mutations in a cysteine-null background (Schulteis et al., 1996; Kobertz et al., 2000). We found two residues

below the S6 bundle crossing (H363C and P369C) and only one residue in the S4–S5 linker (I257C) that formed disulfide bonds with the panel of KCNE1 cysteine mutants. Statistical analysis of cross-link efficiency demonstrated that H363C preferentially reacted with H73C, S74C, and D76C; P369C reacted with D76C only; and I257C was the only residue that had widespread reactivity with the KCNE1 cysteine panel. Functional examination of H363C showed that disulfide bond formation was voltage dependent, occurring predominately when the channel was closed, which was due to two factors: formation of a disulfide bond with E1 and also with a neighboring H363C subunit within the channel complex. Using these experimental constraints, we built a closed-state model of the Q1–E1 cytoplasmic region that positions the E1 C-terminal domain adjacent to the activation gate machinery, which suggests that these protein–protein interactions may slow the opening of the Q1–E1 complex.

MATERIALS AND METHODS

Plasmids and cDNAs
To create cysteine-less (cys−) constructs, wild-type hKCNQ1 and hKCNE1 (containing an extracellularly exposed hemagglutinin A [HA] tag [YPYDVPDYA]) (Wang and Goldstein, 1995), were mutated by Quikchange (Agilent Technologies) site-directed mutagenesis and traditional cassette mutagenesis to remove all native cysteines. Cysteines were either mutated to serine (aqueous) or alanine (membrane embedded) based on a sequence alignment with rKv1.2. The cys− constructs were subcloned into pcDNA3.1(−) mammalian vectors (Invitrogen). Both cDNAs were fully sequenced, and the cysteine-less Q1 channels and Q1–E1 complexes were tested for wild-type voltage-dependent gating and inactivation kinetics.

Cell culture and transfections
Chinese hamster ovary (CHO)-K1 cells were cultured in F-12K nutrient mixture (Invitrogen) supplemented with 10% fetal bovine serum (Hyclone) and 10^2 U/ml penicillin/streptomycin (Invitrogen) and transiently transfected at 70–85% confluency with Lipofectamine (Invitrogen) in Opti-MEM (Invitrogen). DNA ratios were as follows (in µg): Q1/E1 or Q1-cys/E1-cys (Western blots), 0.75:1.5; Q1/E1-cys or Q1-cys/E1-cys (electrophysiology), 0.375:3; Q1 or Q1-cys alone, or Q1/E1 (electrophysiology), 0.75:1.5. For electrophysiology, 0.25 µg of pEGFP-C3 per dish was added. Cells were used 48 h after transfection for Western blots and 24–48 h after transfection for electrophysiological experiments.

Cross-linking in hypotonically lysed cells
For most of the H_2O_2-mediated cross-linking experiments, CHO-K1 cells expressing Q1 and E1 mutants were harvested at 4°C by scraping in 250 µl/well of hypotonic lysis solution (in mM: 10 KCl, 1.5 $MgCl_2$, and 10 HEPES, pH 8.0), supplied with protease inhibitors (1 mM PMSF [EM Science] and 1 µg/ml each of leupeptin [Roche], pepstatin [Roche], and aprotinin [Sigma-Aldrich]). Membranes were pelleted at 10,000 rpm in microcentrifuge for 10 min, resuspended in hypotonic lysis solution, and reduced with 10 mM dithiothreitol (DTT) for 10 min. Membranes were then pelleted (at 10,000 rpm for 10 min at 4°C), washed once in hypotonic lysis solution, resuspended again in hypotonic lysis solution, and oxidized

with a total of 0.01% H_2O_2 for 10 min at room temperature. Unoxidized cysteines were quenched with 30 mM N-ethyl maleimide at room temperature for 1 h. Membranes were once again pelleted (at 10,000 rpm for 10 min at 4°C), removing the supernatant, and solubilized by rolling for 30 min at 4°C in 1.5% digitonin (EMD) solution (in mM: 290 NaCl, 10 KCl, 1 $MgCl_2$, 7 Tris, pH 7.5, and 1.5% digitonin, supplied with protease inhibitors). Proteins were resolved by nonreducing SDS-PAGE and subjected to Western blot analysis. For Q1–Q1 cross-linking experiments, the samples were oxidized with 0.1% H_2O_2, which was the concentration used in electrical recordings. In addition, disulfide bond formation was confirmed by reduction with 50 mM tris(2-carboxyethyl)phosphine for 30 min at 37°C. For the cross-linking of the cell surface labeling proteins, harvest, oxidation, and quench of the membrane proteins were performed as explained above, except that before the cell lysis, their surfaces were biotinylated with EZ-Link sulfo-NHS-SS-biotin (Thermo Fisher Scientific) as described previously (Chandrasekhar et al., 2006).

Coimmunoprecipitation

Harvest, oxidation, and quench of membrane proteins proceeded exactly as described above, except that samples were oxidized with a total of 0.1% H_2O_2. After quenching, membranes were solubilized in RIPKA (in mM: 140 NaCl, 10 KCl, 1% Triton X-100, 0.1% SDS, 1% sodium deoxycholate, 10 Tris-HCl, pH 7.4, and 1 EDTA, pH 8.0, supplied with protease inhibitors), by rolling for 30 min at 4°C). Solubilized proteins were then diluted with 10% (vol/vol) 500 mM Na_3PO_4, pH 7.5, and deglycosylated with ~1% peptide N-glycosidase F (PNGase F; New England Biolabs, Inc.) or mock treated for 1 h at 37°C. After deglycosylation, samples were incubated rolling with ~7.1% (vol/vol) α-Q1 (Santa Cruz Biotechnology, Inc.) overnight at 4°C. Antibody was then bound to immobilized protein G beads (Thermo Fisher Scientific), washed three times with RIPKA, and eluted from beads using a DTT elution solution (in mM: 140 NaCl, 10 Tris, pH 7.4, 1 EDTA, pH 8.0, 100 DTT, and 1% SDS). Finally, the immunoprecipitated samples were resolved by SDS-PAGE, and then subjected to immunoblotting analysis with rat α-HA (Roche) antibody.

Perforated patch whole cell recordings

Currents were recorded in the standard whole cell perforated patch configuration at room temperature (24 ± 2°C). In brief, on the day of the experiment cells were seeded on the surface of cover glass and placed to a custom recording bath filled with a modified Tyrode's solution, which contained (in mM): 145 NaCl, 5.4 KCl, 10 HEPES, and 5 $CaCl_2$, pH 7.5 with NaOH. Transfected (eGFP-expressing) cells were selected using an inverted light microscope (Axiovert 40 CFL; Carl Zeiss, Inc.). For the perforated patch configuration, a glass electrode (pipette resistance: 2.5–3.5 MΩ) was filled with electrode solution (in mM: 126 KCl, 1 $MgSO_2$, 0.5 $CaCl_2$, 5 EGTA, 4 K_2-ATP, 0.4 GTP, and 25 HEPES, pH 7.5 with CsOH), and 60 µg/ml amphotericin B (prepared in DMSO; Sigma-Aldrich) was attached to the cell. Once a GΩ seal was achieved and access resistance was dropped to the sufficient level to record membrane potential (<10 MΩ), Tyrode's solution was replaced with the extracellular bath solution, which contained (in mM): 160 NaCl, 2.5 KCl, 2 $CaCl_2$, 1 $MgCl_2$, 8 glucose, and 10 HEPES, pH 7.5 with NaOH. Initially, the electrical access to the inside of the cell was monitored using a 3-s depolarizing test pulse from the holding potential of −80 to +20 mV taken every 15 s. Prediction, correction, and leak subtraction were not used in any recordings; cells with pronounced rundown were discarded, and only recordings with stable currents were used. Wild-type and cysteine-less Q1 and I_{Ks} were assayed for native function using a "family" protocol, in which cells held at −80 mV were stepped every 15 s to potentials between −100 and +60 mV in 20-mV increments for 3 s, followed by a 1-s tail pulse to −30 mV. H_2O_2-mediated disulfide

bond formation was monitored by holding cells at −80 mV and recording the average current during a 40-ms window at the end of a 20-mV, 3-s test depolarization taken every 15 s. To measure the rate of disulfide bond formation primarily in the closed state, the 3-s test depolarizations were taken every 100 s (instead of 15 s) and compared with the standard protocol. In contrast, open-state oxidation was analyzed using three consecutive 90-s test depolarizations spaced by 100 s at the holding potential (−80 mV); recording solution containing 0.1% H_2O_2 was started at the beginning of either the first inter pulse interval or the second depolarizing pulse.

Data analysis (biochemistry)

Absorbance data for each Western blot was collected using a CCD camera in the linear range, corrected for background noise, and normalized using the equation:

$$y = \frac{abs_{150kD}}{abs_{150kD} + abs_{37-50kD}}.$$

To quantitate the array of bands at 37–50 kD, we measured the entire signal in this range for each sample and subtracted the background intensity from a negative control lane. The normalized absorbance was then plotted as a function of the position of each cysteine mutation (or lack of cysteine mutation) in KCNE1 using Origin 6 software (OriginLab). Statistical significance was determined in two steps. A model of all absorbance data was calculated, and model residuals were collected. The natural logarithm of the calculated residuals fit well to a normal distribution (the Kolmogorov-Smirnov Z value was reduced twofold by taking the natural logarithm, $Z \approx 1.6$). The natural logarithm of each normalized absorbance was subsequently used in a general linear mixed model (Tukey-Kramer) to determine an adjusted p-value. Each experimental set was tested against three negative controls (cross-link between E1 cysteine point mutations and two non-labile cysteine point mutations in Q1 and an internal negative control in each dataset: E1-cys cross-linked with cysteine point mutations in Q1). Only those experimental datasets displaying an adjusted $P < 0.05$ for all three negative controls are labeled. These data are binned according to the least significant p-value.

Data analysis (electrophysiology)

Current normalized to pre-oxidant levels was plotted against time. The resultant time courses of oxidant-induced current reduction fit well to single τ–exponential decay.

Online supplemental material

Fig. S1 contains the quantification of the biochemical cross-linking for all of the Q1–E1 cysteine pairs that were not statistically significant. Fig. S2 compares the oxidation-induced current reduction of H363C to Q1-cys, P369C, and I257C, which were relatively unaffected by oxidant. Fig. S3 A shows that Q1–Q1 cross-link formation with the panel of Q1 mutants was minimal compared with H363C. Fig. S3 B confirms that Q1–E1 cross-link formation occurs at the plasma membrane and was reversible by reductant. Figs. S1–S3 are available at http://www.jgp.org/cgi/content/full/jgp.200910386/DC1.

RESULTS

To biochemically screen the cytoplasmic Q1 residues against residues in the E1 C-terminal domain by disulfide cross-linking (Fig. 1 A), we first removed the native cysteines from the complex because mild oxidation of wild-type

Q1–E1 resulted in higher molecular weight cross-linked species (not depicted). Transient transfection of these cysteine-less versions (Q1-cys and E1-cys) into CHO cells gave rise to currents (Fig. 1 B) with wild-type gating kinetics for both Q1 (fast activation and voltage-dependent inactivation) and Q1–E1 (slow activation/deactivation with no observable inactivation). The cysteine-less Q1–E1 complex did have three behaviors that were of note: (1) the voltage sensitivity of the complex was slightly left-shifted compared with wild type; (2) current expression was more robust compared with wild type; and (3) the current recordings were not stable in the whole cell patch configuration and required the use of the perforated patch technique (see Materials and methods). Notwithstanding
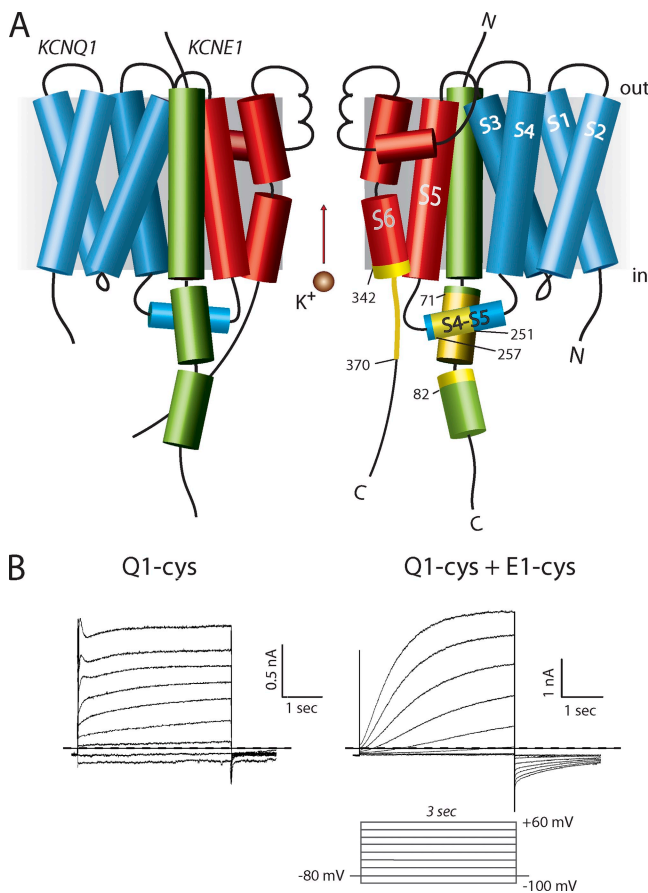

Figure 1. TM topology diagram of the Q1–E1 channel complex highlighting (with yellow) the residues within the juxtamembranous C-terminal domain of E1 and the cytoplasmic face of the Q1 pore domain examined with cysteine cross-linking. (A) For the clarity, only two subunits of the Q1 tetramer are shown. Voltage-sensing and pore-forming domains, and the S4–S5 linker are colored red, blue, and cyan, respectively; E1 is colored green. (B) Cysteine-less Q1 and E1 subunits (−cys) give rise to native-like currents. Representative whole cell currents recorded from CHO-K1 cells transiently transfected with Q1-cys alone (left) or E1-cys (right). Dashed line indicates 0 net current. (Inset) Voltage pulse protocol used to elicit the currents. Membranes were held at −80 mV and stepped to potentials between −100 and +60 mV in 20-mV increments for 3 s; interpulse duration was 15 s.

these subtle differences, the cysteine-less Q1–E1 complex generated the characteristic cardiac I_{Ks} current, indicating that the complex possessed a native-like structure, which we subsequently probed with disulfide cross-linking.

Disulfide bonds form between cysteine residues in the E1 C-terminal domain and the Q1 activation gate machinery

Based on the proposed propinquity of the E1 TM domain and pore domain, we first targeted Q1 residues (342–371), starting at the putative bundle crossing ("PAG") of the S6 activation gate (Seebohm et al., 2006) and ending before the calmodulin binding motif (Shamgar et al., 2006). Because of the dynamic nature of the channel's gate, we did not expect to reveal discrete interactions between amino acid side chains, but rather swathes of E1 cross-linking at certain Q1 residues. The residues in this region were individually mutated to cysteine and separately coexpressed with the panel of E1 C-terminal cysteine mutants (70–82). After 48 h of expression in CHO cells, the reducing intracellular environment was removed by hypotonic lysis, and the lysate was oxidized with hydrogen peroxide (0.01%) for 10 min. The quenched cell lysates were detergent solubilized, and the proteins were resolved by nonreducing SDS-PAGE. Fig. 2 A shows representative E1 Western blots from three Q1 activation gate cysteine mutants. On these low percentage polyacrylamide gels, several bands corresponded to monomeric E1. E1 protein with immature N-linked glycans migrated as a single band at the bottom of the gel, whereas the heterogeneity of the maturely glycosylated E1 protein was resolved as multiple bands between 37 and 50 kD. These bands were not due to E1–E1 cross-links because they were also present in the cysteine-less construct ((−) lane) and in unoxidized samples (not depicted). Although this banding pattern was unaesthetic, it demonstrated that the Q1 and E1 mutants efficiently formed complexes because unpartnered E1 subunits primarily reside in the endoplasmic reticulum with immature glycans (Chandrasekhar et al., 2006). For the H363C and P369C mutants, several other E1-containing species were observed with masses between 50 and 150 kD. Of these higher molecular weight species, the most intense band migrating just below the 150-kD marker had characteristics that were indicative of a cross-link between Q1 and E1; this band required a cysteine in E1, and its intensity was dependent on the position of the cysteine residue.

The intensity of the ~150-kD band was normalized (to the total maturely N-glycosylated E1) and plotted for each E1 residue (Fig. 2 B). As was evident from the blots, the A370C mutant did not significantly react with any residues in the panel of E1 cysteine mutants, whereas the H363C and P369C mutants yielded significant cross-linked material when compared with cysteine-less E1 control ((−) lane). Of all the Q1 cysteine mutants screened (Fig. S1), H363C and P369C were the only two mutants that afforded >20% cross-linking of maturely glycosylated E1 protein.
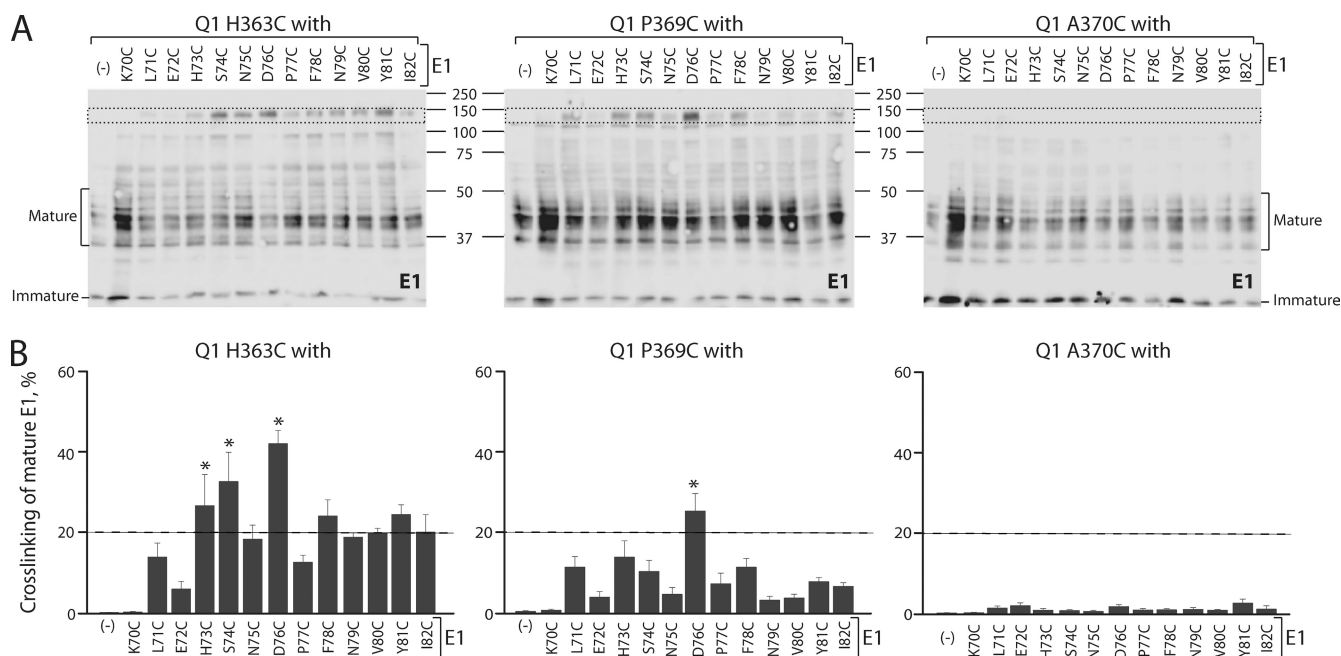
Figure 2. Two Q1 cysteine mutants, H363C and P369C, near the S6 activation gate form higher molecular weight species with a panel of single-cysteine E1 mutants. (A) Western blots from hypotonically lysed CHO cells oxidized with 0.01% H_2O_2 for 10 min. Proteins were resolved on nonreducing SDS-PAGE and immunoblotted for E1. All single-cysteine E1 mutants produce a series of bands between 37 and 50 kD, which corresponded to maturely N-glycosylated E1 peptides; immaturely N-glycosylated E1 is located at the bottom of the blots. Oxidation results in several higher molecular weight species between 50 and 150 kD, with an intense band just below 150 kD (dotted box). The strength of this band varies depending on the identity of the cross-link pairing. Molecular weight and monomeric glycoforms of E1 are denoted. (B) Normalized signal intensity of the ~150-kD Q1–E1 band plotted against the position of the cysteine in E1 for the single-cysteine Q1 mutants showed in A. Signal denotes the mean for $n = 3$–4 experiments ± SEM. Asterisks indicate significance of at least P < 0.01. The dashed line is shown because cross-linking >20% was determined to be statistically significant.

Statistical analysis of the reactive E1 cysteine residues revealed that H73C, S74C, and D76C were significantly more reactive with H363C; and D76C with P369C.

Having found these putative cross-linked species, we sought to determine whether they were composed of a disulfide-bonded Q1–E1 heterodimer. Because Q1–Q1 homodimers (vide infra) have similar mobility on SDS-PAGE, we used denaturing coimmunoprecipitation (Fig. 3 A) to identify the proteins in the cross-link and to determine whether they were covalently attached via a disulfide bond. In this approach, the oxidized cell ghosts were dissolved in SDS to denature the Q1–E1 complexes, and the detergent-solubilized Q1 protein was quantitatively immunoprecipitated (Fig. 3, Q1 blot). Under these denaturing conditions, only E1 protein covalently attached to Q1 subunits will precipitate and be removed from the supernatant. Mild DTT treatment of the immunoprecipitated material selectively breaks the disulfide bond, eluting any covalently attached E1 subunits from bead-bound Q1 subunits. Fig. 3 B shows the results from a denaturing immunoprecipitation between H363C and S74C and D76C. The oxidized input lanes show that the intensity of the band at 150 kD was highly dependent on both subunits containing a cysteine. Denaturing immunoprecipitation of the Q1 subunits selectively precipitated the two intense 150-kD bands, but

the panoply of other bands remained in the supernatant. Elution of the disulfide-bound proteins with DTT only produced an E1 signal when both cysteine residues were present in the Q1–E1 complex. Moreover, PNGase F treatment identified the eluted E1 protein as maturely N-glycosylated, indicating that the cross-linked Q1–E1 complexes were properly folded because they passed the quality control machinery in the endoplasmic reticulum. Thus, the results in Fig. 3 B identify the cross-linked species at ~150 kD as disulfide-bonded Q1–E1 heterodimers with mature N-linked glycosylation and demonstrate that the E1 C-terminal domain interacts with two residues (H363 and P369) below the S6 activation gate.

Because the S4–S5 linker of Q1 communicates voltage sensor movement to the S6 activation gate opening, we next probed this Q1 cytoplasmic linker for interactions with the E1 C-terminal domain. Using our initial oxidation conditions (0.01% H_2O_2), we observed little to no cross-linking between the S4 and S5 residues (251–257) and the E1 C-terminal domain (not depicted). However, increasing the concentration fivefold resulted in broad-spectrum cross-linking between I257C and the panel of E1 cysteine mutants (Fig. 4). Cross-linking was specific for I257C because the other cysteine mutants in the S4–S5 linker remained unreactive with the increase in oxidant concentration (Fig. S1 B).
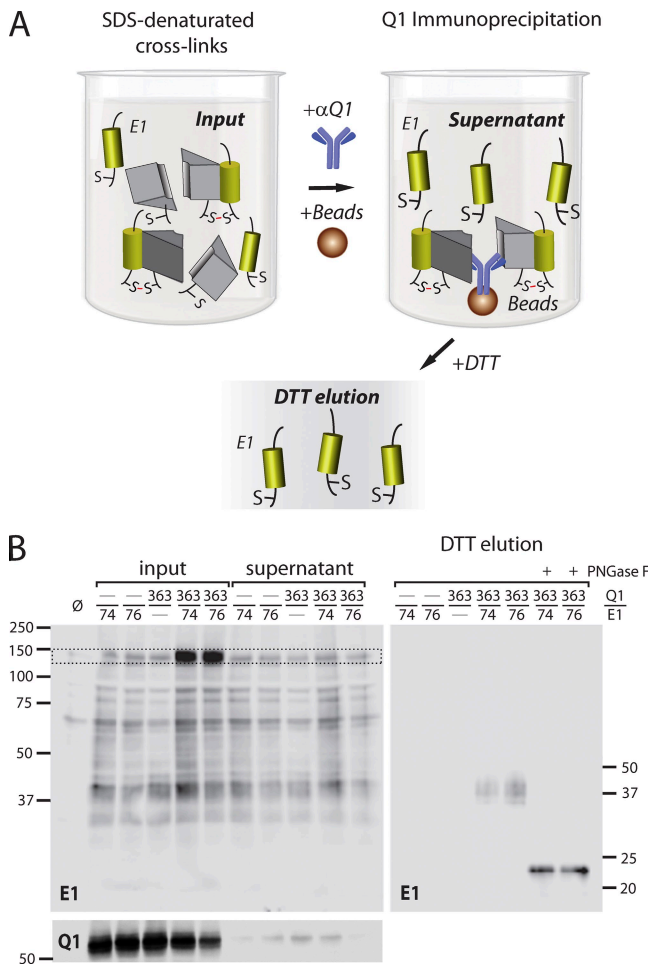
Figure 3. The ~150-kD species are Q1–E1 disulfide-bound heterodimers. (A) Cartoon depiction of the strategy used to verify the protein cross-link of the ~150-kD band. Membrane-embedded proteins were oxidized with 0.1% H_2O_2 for 10 min, dissolved in detergent, and immunoprecipitated with anti-Q1 antibodies. Elution with DTT releases the E1 subunits covalently attached to Q1 subunits via a disulfide bond. (B) Western blots from a denaturing coimmunoprecipitation of oxidized Q1–E1 complexes. (Left) Inputs and supernatants from oxidized whole cell CHO lysates were probed with E1 (top) or Q1 (bottom) Western blot. The protein loaded for each Q1–E1 pairing was kept constant. Cysteine mutants are denoted above blot: −, cysteine-less subunit; Ø, nontransfected cells. Molecular weight markers are shown on the left. E1 blot demonstrates that immunoprecipitation of Q1 removes the ~150-kD band on the E1 blot only when both subunits contain a cysteine (363/74 and 363/76). The Q1 blot shows the efficacy of immunoprecipitation; quantization of the bands showed that >95% of Q1 protein was immunoprecipitated. (Right) DTT elution releases E1 subunits from the immunoprecipitated Q1–E1 complexes only when there is a cysteine in each subunit. The maturely heteroglycosylated E1 proteins run as a smear at ~37 kD (Chandrasekhar et al., 2006). Mature N-linked glycans were removed with PNGase F treatment (+).

Functional consequences of disulfide formation in the Q1 activation gate machinery and E1 C-terminal domain

After identifying pairs of Q1–E1 cysteine mutants that formed disulfide bonds in biochemical experiments, we

determined how oxidation of these complexes would affect function. The different Q1–E1 cysteine pairs were first expressed in CHO cells, and whole cell currents were elicited with a 3-s depolarizing test pulse to +20 mV. Current for all Q1–E1 cysteine pairings exhibited the slow gating kinetics of I_{Ks} and lacked any signs of inactivation, indicating that the mutant subunits properly coassembled (Fig. 5 A and Fig. S2). Oxidative treatment of H363C paired with the more biochemically reactive E1 mutants H73C, S74C, or D76C resulted in 80–90% reduction of current within 5 min (Fig. 5 A, top row). In contrast, the currents from P369C and I257C coexpressed with D76C were relatively unaffected by oxidant (Fig. S2, C–F). Further functional examination of H363C revealed that oxidation reduced the currents regardless of the position of the cysteine in E1 (Fig. S2). Because the single cysteines in E1 expressed with cysteine-less Q1 (Q1-cys) were minimally affected by oxidant (Fig. 5 A, middle row), we suspected that the oxidant was inducing Q1 subunit homodimerization via the H363C residue. Oxidation of H363C expressed with cysteine-less E1 (E1-cys) resulted in 50% reduction of current, which was significant compared with the cysteine-less Q1–E1 complex (Fig. 5 A, bottom row). A comparison of the mutant Q1–E1 complexes (Fig. 5 B) clearly showed that oxidation of H363C was a major contributor to current loss; however, the inclusion of E1 cysteine mutants at positions 73, 74, or 76 also contributed to current reduction. Attempts to reverse the oxidant-induced current inhibition by treating the cells with 2–5 mM DTT consistently resulted in loss of the gigaohm seal within 30 s of application (not depicted). Thus, in functional assays, it was unclear whether a disulfide bond was forming between Q1 subunits.

To directly test for Q1–Q1 disulfide bond formation, we revisited the H363C mutant in biochemical assays (Fig. 5 C). Oxidation of hypotonically lysed cells expressing the cysteine-less Q1–E1 construct afforded primarily monomeric Q1 protein on Western blots, although a faint band migrating at the predicted dimer size was always discernable. In contrast, a strong band was observed when H363C was coexpressed with either D76C or E1-cys, demonstrating that Q1–Q1 dimers were forming in the absence of a cysteine in the E1 subunit. Treatment of the oxidized samples with reductant collapsed the cysteine-specific Q1–Q1 dimer band into a monomer (Fig. 5 C, right), which identified this band as a disulfide bonded Q1 homodimer. Robust disulfide bond formation between Q1 subunits was only observed for H363C, although weaker Q1–Q1 cross-linking was observed for the residues adjacent to H363C (Fig. S3 A).

State-dependent cross-linking of Q1–E1 complexes

Because the H363C mutant mediated Q1–Q1 homodimerization, we next determined whether the cross-link
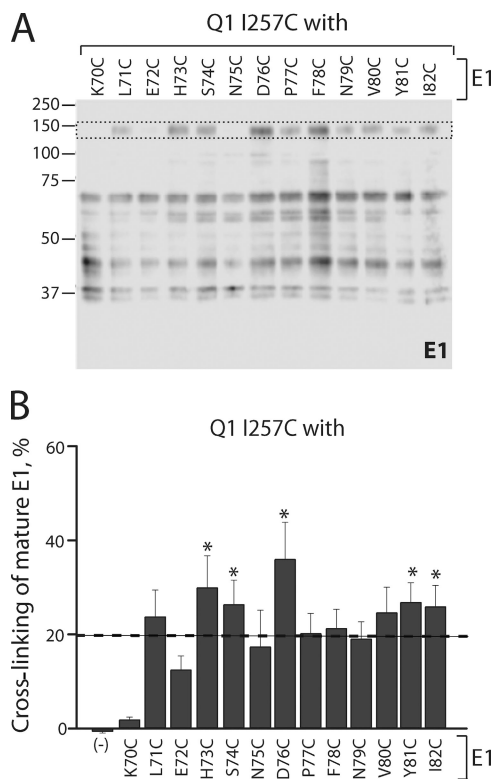
Figure 4. A cysteine mutant (I257C) in the S4–S5 forms cross-links with the panel of E1 cysteine mutants. (A) Western blots from hypotonically lysed CHO cells oxidized with 0.05% H_2O_2 for 10 min. Proteins were resolved on nonreducing SDS-PAGE and immunoblotted for E1. Oxidation results in several higher molecular weight species between 50 and 150 kD, with the previously identified Q1–E1 cross-link just below 150 kD (dotted box). The strength of this band was again dependent on the cross-link pairing. Molecular weight markers are denoted. (B) Normalized signal intensity of the ~150-kD species formed by I257C with a panel of E1 mutants. Bars denote the mean for six experiments ± SEM. Asterisks indicate significance of at least $P < 0.05$. The dashed line is shown because cross-linking >20% was determined to be statistically significant.

formed in the open and/or closed state. To examine cross-linking primarily in the closed state, we compared the rates of oxidant-induced current reduction using two protocols that varied the time spent at depolarizing potentials. The first protocol was our standard protocol, where the cell was depolarized 20% of the time (Fig. 6, inset). The second protocol maximized the time the cell was held at rest with only brief, +20-mV sojourns to measure the effect of oxidant application (Fig. 6, filled circles). Fig. 6 A shows that rates of oxidized-induced current reduction of H363C were similar regardless of the protocol used. Minimizing the number of depolarizations with D76C in the complex had no affect on the rate of current reduction, although its presence did modestly accelerate the rate of current reduction compared with H363C alone (50 ± 10 s vs. 64 ± 16 s). Thus, H363C homodimerization occurs in the closed state, and inclusion

of a cysteine in E1 (D76C) appears to enhance cross-link formation.

Although both the H363C–E1-cys and H363C–D76C complexes efficiently formed cross-links in the closed state, the previous rate comparison experiments did not rule out the possibility that the reaction could also occur in the open state. To directly test for open-state cross-linking, we took advantage of one of the unique properties of the Q1–E1 complex: the complex does not inactivate with prolonged depolarizations (minutes) (Tzounopoulos et al., 1998). On this time scale, it was feasible to apply oxidant to a whole cell during a depolarization versus at rest. Because depolarizing a cell on the minute timescale is a bit unorthodox, we first determined whether we could repetitively depolarize the same cell for 90 s and reproducibly acquire Q1–E1 currents. The black current traces in Fig. 6 B show that three sequential 90-s depolarizations elicited relatively stable currents from the H363C–D76C complex. The application of oxidant during the first inter-depolarization interval (Fig. 6 B, blue data) resulted in a reduction of current in the subsequent depolarization, confirming the closed-state cross-linking in Fig. 6 A. However, the application of oxidant at the start of the second depolarization (Fig. 6 B, red data) had little to no effect on the magnitude of the ending current, indicating that neither the H363C–H363C nor the H363–D76C cross-link appreciably forms in the open state. As expected, closing the channel complex after the second depolarization resulted in rapid cross-link formation that was visualized in the third and final depolarization (Fig. 6, B and C). In total, these state-dependent experiments established that both H363C–H363C and H363–D76C cross-link formation predominately occurs when the complex is closed.

DISCUSSION

Previous Q1–E1 cysteine cross-linking studies have focused on extracellular protein–protein interactions in intact cells, where the environment is oxidizing and the membrane potential of the cell provides control of complex conformation. In the present work, we focused on the juxtamembranous part of the E1 C terminus because this domain adopts a helical structure, where both laboratory-made and long QT mutations cluster to one face of the helix predicted to face the cytoplasmic side of the Q1 channel (Rocheleau et al., 2006). To identify these Q1–E1 protein interactions, we oxidized hypotonically lysed cells, which provided cytoplasmic access to the complex in a membranous environment. Although these conditions enabled us to screen hundreds of pairs of Q1–E1 residues, our approach comes with a caveat: hypotonic lysis destroys the electrochemical gradient and TM potential. Thus, at 0 mV the activation gate machinery of the channel is predicted to be undergoing large movements while equilibrating

between open and closed states. Moreover, there is evidence that the E1 TM domain rotates during gating (Xu et al., 2008; Chung et al., 2009), which if propagated to the C terminus would also promote widespread cross-linking. Accordingly, the reactive Q1 cysteine mutants identified here form cross-links with most of the E1 cysteine mutants studied. In spite of this caveat, we were able to identify three residues in Q1 (H363C, P369C, and I257C) that readily formed disulfide bonds with cysteine residues in the E1 C-terminal domain (Figs. 2 and 4). Statistical analysis demonstrated that there was some selectivity for certain E1 residues: H363C with H73C, S74C, and D76C; P369C with D76C. Based on a previous periodicity analysis of mutation-induced

perturbations of Q1–E1 complex function (Rocheleau et al., 2006), these three residues are predicted to face the Q1 channel. Although not statistically significant, visual inspection of the biochemical reactivity of the E1 cysteine mutants uncannily mirrors the previously studied functionally disruptive alanine mutants: 73, 74, 76, 78, 81, and 82. Given that the cross-linked Q1–E1 subunits arose from Q1–E1 complexes that were properly folded (presence of mature glycosylation; Figs. 2–4) with I_{Ks} kinetics (Fig. 5 A and Fig. S2), and at the cell surface (Fig. S3 B), we conclude that these mutant Q1–E1 complexes have maintained their wild-type structure. Thus, our data show that the E1 C-terminal domain forms a protein–protein interaction with
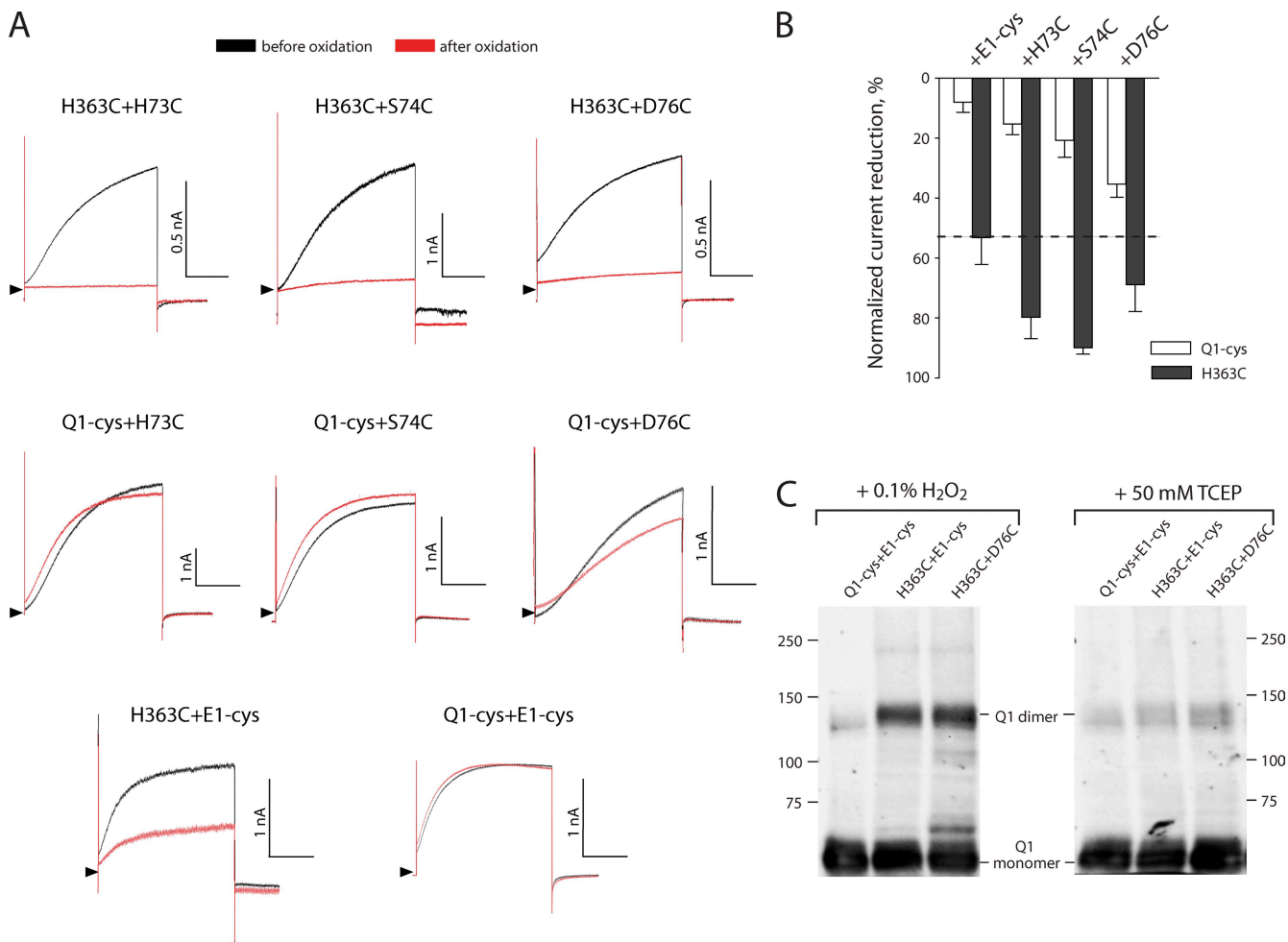

Figure 5. Oxidant-mediated cross-linking at H363C results in a disulfide bond between adjacent Q1 subunits. (A) Whole cell currents observed in CHO cells for (top) H363C with three E1 cysteine mutants, (middle) Q1-cys with three E1 cysteine mutants, and (bottom) H363C with E1-cys and the cysteine-less complex (Q1-cys+E1-cys). Black traces are before oxidation, and red traces are after a 5-min treatment with oxidant (0.1% H_2O_2). Currents were elicited by a 3-s depolarizing step from the holding potential of −80 to +20 mV with a 12-s interpulse interval. 0 current is labeled with a triangle, and the scale bar denotes 1 s. (B) Normalized oxidant-induced current reduction of the panel of Q1–E1 cysteine mutants. Currents measured before and after the oxidation were normalized and plotted as mean ± SEM; n = 3–6 samples per pairing. (C) H363C forms Q1–Q1 homodimers in the presence or absence of an E1 cysteine residue. CHO cells expressing the different Q1–E1 complexes were lysed, treated with peroxide, separated on nonreducing SDS-PAGE, and subjected to Western blot analysis using anti-Q1 antibodies. A band corresponding to a covalent dimer of H363C subunits was observed with or without D76C in the complex (left). The dimeric entities could be disassembled into monomer by reduction with tris(2-carboxyethyl)phosphine (TCEP; right).

Q1 residues below the S6 activation gate and in the S4–S5 linker.

Surprisingly, oxidation of two of the biochemically reactive Q1 cysteine residues (P369C and I257C) in whole cell recordings had no measurable effect on Q1–E1 complex function when paired with a reactive E1 cysteine mutant (Fig. S2, C–F). Lack of functional phenotype for these two Q1 mutants may be due to diminished reactivity of peroxide in the reducing environment of the cell, even though we increased the concentration 10-fold for these intact cell experiments. It is also possible that these two Q1 residues are indeed forming a cross-link with the E1 subunit, but the disulfide bond does not hinder the voltage gating

of the complex, and thus function is unaffected. A similar functionally non-disruptive cross-link hypothesis has been proposed for extracellular biochemical cross-links that do not perturb Q1–E1 function (Chung et al., 2009).

In contrast to P369C and I257C, we observed rapid loss of function when H363C was in the Q1–E1 complex. However, the extent of oxidant-induced current inhibition for H363C was similar for all of the E1 cysteine mutants—even for residues that showed minimal reactivity in biochemical experiments (Fig. 5 and Fig. S2 A). This across the board loss of function suggested that H363C was forming an inter Q1 subunit cross-link, which we confirmed with the H363C–E1-cys complex in electrical
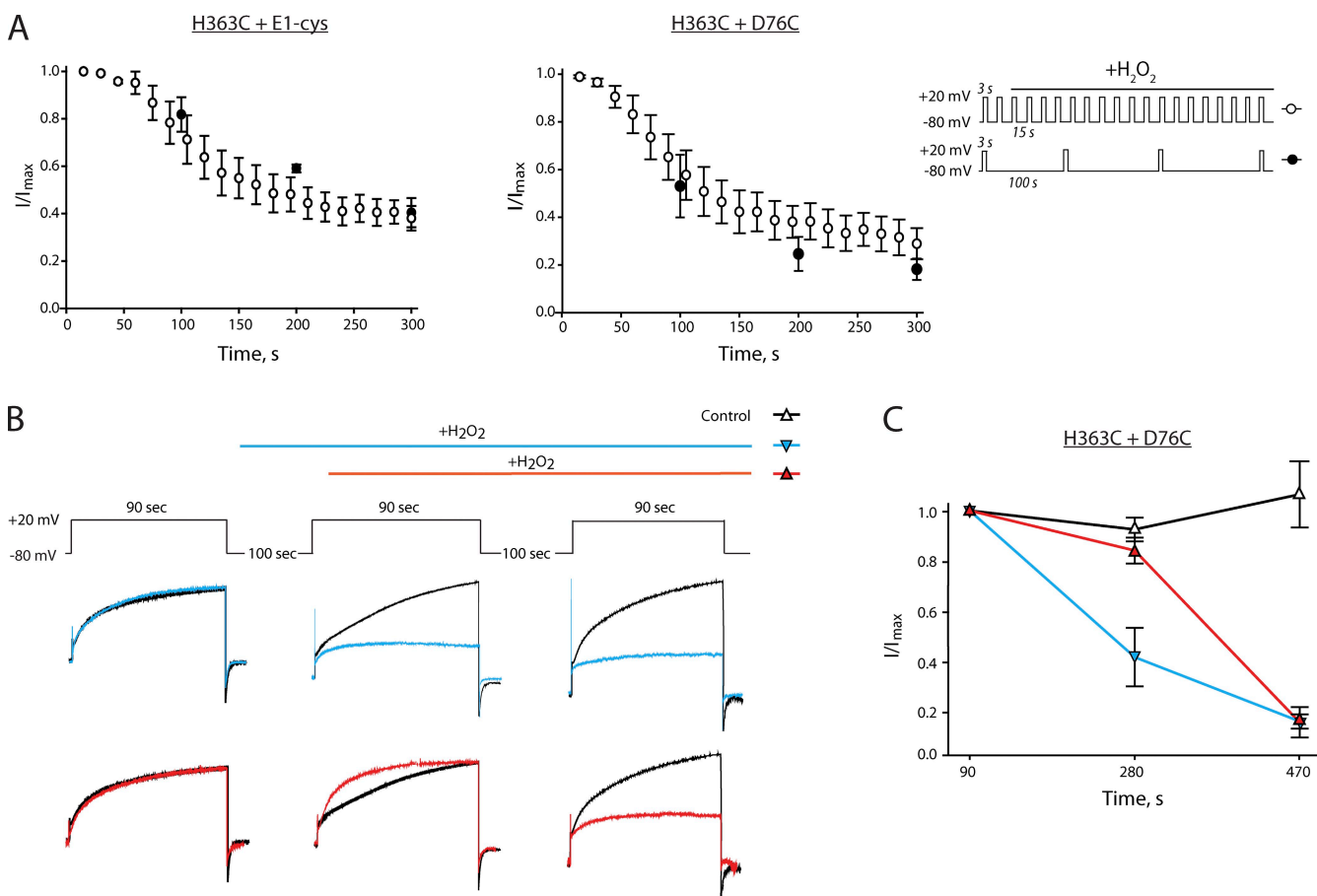

Figure 6. Q1–Q1 cross-link formation via H363C predominately occurs in the closed state. (A) Change in current monitored over time using +20-mV test pulses with a different interpulse duration, as shown in inset. Open circles represent the "open-state" protocol, where channels were depolarized 20% of total time (3-s pulse every 15 s), and filled circles are for "closed-state" protocol, where channels were depolarized 4% of total time (3-s pulse every 100 s). Recordings are from CHO cells expressing H363C with either E1-cys or D76C. Clamped cells exhibiting stable currents were exposed to perfusion of 0.1% H_2O_2, as shown in the inset. Data points are mean ± SEM ($n = 3$). Time constants of oxidant-induced inhibition: H363C alone, 64 ± 16 s; H363C/D76C, 50 ± 10 s. (B) Application of oxidant to complexes at resting and depolarizing potentials. Currents were elicited using 90-s depolarizing pulses to +20 mV separated by 100-s interpulse intervals at a resting potential of −80 mV. Hydrogen peroxide (0.1%) was applied at either the start of the first interpulse interval (blue) or the beginning of the second depolarizing test pulse (blue). Control traces (no peroxide applied) are shown in black. Oxidation during an interpulse interval results in an immediate loss of current, whereas oxidation at depolarizing potential (+20 mV) for the same duration has little to no effect on the magnitude of the current measured at the end of the depolarization. (C) Reduction of current over time for the different oxidation conditions. Current values were measured at the end of each +20-mV test pulse and are plotted as mean ± SEM ($n = 3$).

recordings and nonreducing SDS-PAGE (Fig. 5). Although the Q1–Q1 cross-link accounted for most of the current inhibition observed with H363C, inclusion of certain E1 cysteine mutants in the complex increased the amount of oxidized-induced current inhibition (Fig. 5 and Fig. S2 A). Whether this additional reduction of current is due to a direct Q1–E1 cross-link (as was observed in biochemical experiments) or an E1 cysteine–mediated acceleration of Q1–Q1 cross-link formation is uncertain. Nonetheless, either mechanism requires the E1 cysteine residue to be spatially close to the H363C residue.

Because oxidation-induced inhibition of H363C could be monitored in whole cell recordings, we compared the rates of inhibition using two different voltage pulse protocols to determine whether cross-link formation was occurring in a state-dependent manner (Fig. 6). By exploiting the unusual gating kinetics of the Q1–E1 complex (slow activation and lack of inactivation at depolarizing potentials), we showed in intact cells that H363C predominately formed a cross-link in the closed state. Inclusion of a cross-linkable cysteine in E1 (D76C) into the complex did not change the state dependency of oxidant-induced inhibition of H363C. Thus, from these state-dependent experiments, we conclude that the H363C residues are adjacent to each other when the Q1 activation gate is closed, and D76 in E1 is also near the cytoplasmic gate in the closed state.

Using these experimental results, we generated a closed-state model of the Q1–E1 cytoplasmic region (Fig. 7). We fashioned our model from the predicted three-dimensional structural model of the human Q1 channel in the closed conformation (Smith et al., 2007) and the NMR structure of E1 TM domain reconstituted in lyso-myristoylphosphatidylglycerol micelles (Kang et al., 2008). Unfortunately, neither structure possesses the data to model the Q1 and E1 cytoplasmic domains in their native conformation. Therefore, we propagated the TM helices of Q1 and E1 until we reached beyond the regions of interest. For the juxtamembranous part of the E1 C terminus, we chose to introduce a kink at E1 residue P77 because we have previously shown that this domain is either a proline-kinked helix or a helix that experiences two different protein–protein interactions (Rocheleau et al., 2006). To create the model of the Q1–E1 cytoplasmic region, we positioned the E1 C-terminal domain adjacent to the Q1 activation gate machinery, such that D76C, the most reactive E1 residue, was centrally located while keeping the E1 TM domain close to the S6, S1, and S4 helices of Q1 (Xu et al., 2008; Chung et al., 2009). Because the cytoplasmic domains are not based on crystallographic data or NMR restraints, no computer simulations or docking were used; however, a visual inspection of the superimposed structures was performed to ex-

clude any imposition of van der Waals volumes. Only one of the two E1 subunits is shown in Fig. 7 (H. Chen et al., 2003; Morin and Kobertz, 2008). The model provocatively intimates that the E1 C-terminal domains may encumber the Q1 activation gate machinery, slowing down the transition from closed to open and leading to the generation of the cardiac I_{Ks} current. If our model is operational, the slowed activation of Q1–E1 complexes could arise from either the specific Q1–E1 interactions identified here, or by non-specific obstruction of activation gate opening by the E1 C terminus.
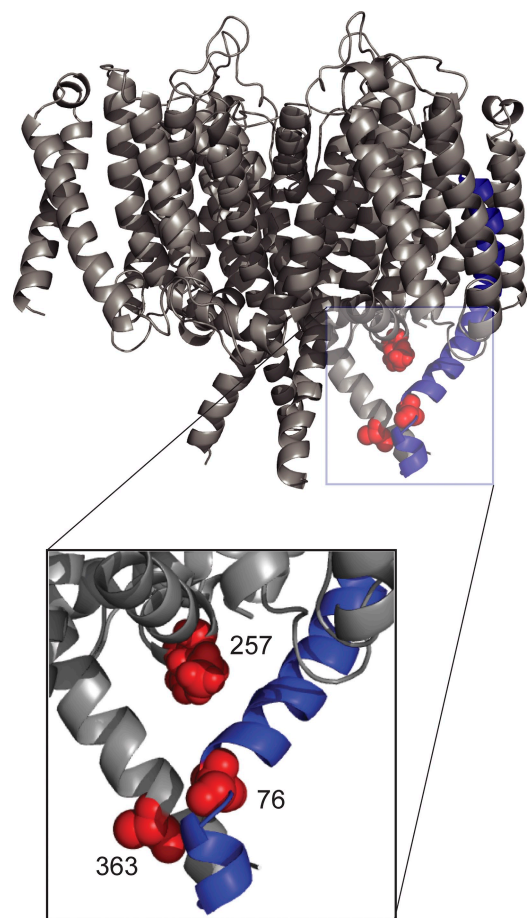
Figure 7. Cartoon model depicting the cytoplasmic interactions of the E1 C-terminal domain and the Q1 activation gate machinery. (Inset) Magnification of the region of interest depicting the residues identified by cysteine cross-linking. Q1 subunits are gray, E1 subunit is blue, and the indentified residues are red and rendered as space-fill.

REFERENCES

Barhanin, J., F. Lesage, E. Guillemare, M. Fink, M. Lazdunski, and G. Romey. 1996. K_VLQT1 and IsK (minK) proteins associate to form the I_{Ks} cardiac potassium current. *Nature.* 384:78–80. doi:10.1038/384078a0

Chandrasekhar, K.D., T. Bas, and W.R. Kobertz. 2006. KCNE1 subunits require co-assembly with K^+ channels for efficient trafficking and cell surface expression. *J. Biol. Chem.* 281:40015–40023. doi:10.1074/jbc.M604398200

Chen, H., L.A. Kim, S. Rajan, S. Xu, and S.A. Goldstein. 2003. Charybdotoxin binding in the $I_{(Ks)}$ pore demonstrates two MinK subunits in each channel complex. *Neuron.* 40:15–23. doi:10.1016/S0896-6273(03)00570-1

Chen, Y.H., S.J. Xu, S. Bendahhou, X.L. Wang, Y. Wang, W.Y. Xu, H.W. Jin, H. Sun, X.Y. Su, Q.N. Zhuang, et al. 2003. KCNQ1 gain-of-function mutation in familial atrial fibrillation. *Science.* 299:251–254. doi:10.1126/science.1077771

Chouabe, C., N. Neyroud, P. Guicheney, M. Lazdunski, G. Romey, and J. Barhanin. 1997. Properties of KvLQT1 K+ channel mutations in Romano-Ward and Jervell and Lange-Nielsen inherited cardiac arrhythmias. *EMBO J.* 16:5472–5479. doi:10.1093/emboj/16.17.5472

Chung, D.Y., P.J. Chan, J.R. Bankston, L. Yang, G. Liu, S.O. Marx, A. Karlin, and R.S. Kass. 2009. Location of KCNE1 relative to KCNQ1 in the I(KS) potassium channel by disulfide cross-linking of substituted cysteines. *Proc. Natl. Acad. Sci. USA.* 106:743–748. doi:10.1073/pnas.0811897106

Gage, S.D., and W.R. Kobertz. 2004. KCNE3 truncation mutants reveal a bipartite modulation of KCNQ1 K^+ channels. *J. Gen. Physiol.* 124:759–771. doi:10.1085/jgp.200409114

Haitin, Y., R. Wiener, D. Shaham, A. Peretz, E.B. Cohen, L. Shamgar, O. Pongs, J.A. Hirsch, and B. Attali. 2009. Intracellular domains interactions and gated motions of I(KS) potassium channel subunits. *EMBO J.* 28:1994–2005. doi:10.1038/emboj.2009.157

Hong, K., D.R. Piper, A. Diaz-Valdecantos, J. Brugada, A. Oliva, E. Burashnikov, J. Santos-de-Soto, J. Grueso-Montero, E. Diaz-Enfante, P. Brugada, et al. 2005. De novo KCNQ1 mutation responsible for atrial fibrillation and short QT syndrome in utero. *Cardiovasc. Res.* 68:433–440. doi:10.1016/j.cardiores.2005.06.023

Kang, C., C. Tian, F.D. Sönnichsen, J.A. Smith, J. Meiler, A.L. George Jr., C.G. Vanoye, H.J. Kim, and C.R. Sanders. 2008. Structure of KCNE1 and implications for how it modulates the KCNQ1 potassium channel. *Biochemistry.* 47:7999–8006. doi:10.1021/bi800875q

Kobertz, W.R., C. Williams, and C. Miller. 2000. Hanging gondola structure of the T1 domain in a voltage-gated $K^{(+)}$ channel. *Biochemistry.* 39:10347–10352. doi:10.1021/bi001292j

Lai, L.P., Y.N. Su, F.J. Hsieh, F.T. Chiang, J.M. Juang, Y.B. Liu, Y.L. Ho, W.J. Chen, S.J. Yeh, C.C. Wang, et al. 2005. Denaturing high-performance liquid chromatography screening of the long QT syndrome-related cardiac sodium and potassium channel genes and identification of novel mutations and single nucleotide polymorphisms. *J. Hum. Genet.* 50:490–496. doi:10.1007/s10038-005-0283-3

Lundby, A., L.S. Ravn, J.H. Svendsen, S.P. Olesen, and N. Schmitt. 2007. KCNQ1 mutation Q147R is associated with atrial fibrillation and prolonged QT interval. *Heart Rhythm.* 4:1532–1541. doi:10.1016/j.hrthm.2007.07.022

Ma, L., C. Lin, S. Teng, Y. Chai, R. Bähring, V. Vardanyan, L. Li, O. Pongs, and R. Hui. 2003. Characterization of a novel Long QT syndrome mutation G52R-KCNE1 in a Chinese family. *Cardiovasc. Res.* 59:612–619. doi:10.1016/S0008-6363(03)00510-8

Mall, M., A. Wissner, R. Schreiber, J. Kuehr, H.H. Seydewitz, M. Brandis, R. Greger, and K. Kunzelmann. 2000. Role of K(V)LQT1 in cyclic adenosine monophosphate-mediated Cl(-) secretion in human airway epithelia. *Am. J. Respir. Cell Mol. Biol.* 23:283–289.

McCrossan, Z.A., and G.W. Abbott. 2004. The MinK-related peptides. *Neuropharmacology.* 47:787–821. doi:10.1016/j.neuropharm.2004.06.018

Melman, Y.F., S.Y. Um, A. Krumerman, A. Kagan, and T.V. McDonald. 2004. KCNE1 binds to the KCNQ1 pore to regulate potassium channel activity. *Neuron.* 42:927–937. doi:10.1016/j.neuron.2004.06.001

Morin, T.J., and W.R. Kobertz. 2008. Counting membrane-embedded KCNE β-subunits in functioning K^+ channel complexes. *Proc. Natl. Acad. Sci. USA.* 105:1478–1482. doi:10.1073/pnas.0710366105

Napolitano, C., S.G. Priori, P.J. Schwartz, R. Bloise, E. Ronchetti, J. Nastoli, G. Bottelli, M. Cerrone, and S. Leonardi. 2005. Genetic testing in the long QT syndrome: development and validation of an efficient approach to genotyping in clinical practice. *JAMA.* 294:2975–2980. doi:10.1001/jama.294.23.2975

Neyroud, N., F. Tesson, I. Denjoy, M. Leibovici, C. Donger, J. Barhanin, S. Fauré, F. Gary, P. Coumel, C. Petit, et al. 1997. A novel mutation in the potassium channel gene KVLQT1 causes the Jervell and Lange-Nielsen cardioauditory syndrome. *Nat. Genet.* 15:186–189. doi:10.1038/ng0297-186

Nicolas, M., D. Demêmes, A. Martin, S. Kupershmidt, and J. Barhanin. 2001. KCNQ1/KCNE1 potassium channels in mammalian vestibular dark cells. *Hear. Res.* 153:132–145. doi:10.1016/S0378-5955(00)00268-9

Panaghie, G., K.K. Tai, and G.W. Abbott. 2006. Interaction of KCNE subunits with the KCNQ1 K+ channel pore. *J. Physiol.* 570:455–467. doi:10.1113/jphysiol.2005.100644

Rocheleau, J.M., S.D. Gage, and W.R. Kobertz. 2006. Secondary structure of a KCNE cytoplasmic domain. *J. Gen. Physiol.* 128:721–729. doi:10.1085/jgp.200609657

Roepke, T.K., A. Anantharam, P. Kirchhoff, S.M. Busque, J.B. Young, J.P. Geibel, D.J. Lerner, and G.W. Abbott. 2006. The KCNE2 potassium channel ancillary subunit is essential for gastric acid secretion. *J. Biol. Chem.* 281:23740–23747. doi:10.1074/jbc.M604155200

Sanguinetti, M.C., and N.K. Jurkiewicz. 1990. Two components of cardiac delayed rectifier K^+ current. Differential sensitivity to block by class III antiarrhythmic agents. *J. Gen. Physiol.* 96:195–215. doi:10.1085/jgp.96.1.195

Sanguinetti, M.C., M.E. Curran, A. Zou, J. Shen, P.S. Spector, D.L. Atkinson, and M.T. Keating. 1996. Coassembly of $K_{(V)}$LQT1 and minK (IsK) proteins to form cardiac $I_{(Ks)}$ potassium channel. *Nature.* 384:80–83. doi:10.1038/384080a0

Schroeder, B.C., S. Waldegger, S. Fehr, M. Bleich, R. Warth, R. Greger, and T.J. Jentsch. 2000. A constitutively open potassium channel formed by KCNQ1 and KCNE3. *Nature.* 403:196–199. doi:10.1038/35003200

Schulteis, C.T., N. Nagaya, and D.M. Papazian. 1996. Intersubunit interaction between amino- and carboxyl-terminal cysteine residues in tetrameric shaker K+ channels. *Biochemistry.* 35:12133–12140. doi:10.1021/bi961083s

Schulze-Bahr, E., M. Schwarz, S. Hauenschild, H. Wedekind, H. Funke, W. Haverkamp, G. Breithardt, O. Pongs, D. Isbrandt, and S. Hoffman. 2001. A novel long-QT 5 gene mutation in the C-terminus (V109I) is associated with a mild phenotype. *J. Mol. Med.* 79:504–509. doi:10.1007/s001090100249

Seebohm, G., N. Strutz-Seebohm, O.N. Ureche, R. Baltaev, A. Lampert, G. Kornichuk, K. Kamiya, T.V. Wuttke, H. Lerche, M.C. Sanguinetti, and F. Lang. 2006. Differential roles of S6 domain hinges in the gating of KCNQ potassium channels. *Biophys. J.* 90:2235–2244. doi:10.1529/biophysj.105.067165

Shamgar, L., L. Ma, N. Schmitt, Y. Haitin, A. Peretz, R. Wiener, J. Hirsch, O. Pongs, and B. Attali. 2006. Calmodulin is essential for cardiac IKS channel gating and assembly: impaired function in long-QT mutations. *Circ. Res.* 98:1055–1063. doi:10.1161/01.RES.0000218979.40770.69

Smith, J.A., C.G. Vanoye, A.L. George Jr., J. Meiler, and C.R. Sanders. 2007. Structural models for the KCNQ1 voltage-gated potassium channel. *Biochemistry*. 46:14141–14152. doi:10.1021/bi701597s

Splawski, I., K.W. Timothy, G.M. Vincent, D.L. Atkinson, and M.T. Keating. 1997a. Molecular basis of the long-QT syndrome associated with deafness. *N. Engl. J. Med.* 336:1562–1567. doi:10.1056/NEJM199705293362204

Splawski, I., M. Tristani-Firouzi, M.H. Lehmann, M.C. Sanguinetti, and M.T. Keating. 1997b. Mutations in the hminK gene cause long QT syndrome and suppress IKs function. *Nat. Genet.* 17:338–340. doi:10.1038/ng1197-338

Splawski, I., J. Shen, K.W. Timothy, M.H. Lehmann, S. Priori, J.L. Robinson, A.J. Moss, P.J. Schwartz, J.A. Towbin, G.M. Vincent, and M.T. Keating. 2000. Spectrum of mutations in long-QT syndrome genes. KVLQT1, HERG, SCN5A, KCNE1, and KCNE2. *Circulation*. 102:1178–1185.

Tai, K.K., and S.A. Goldstein. 1998. The conduction pore of a cardiac potassium channel. *Nature*. 391:605–608. doi:10.1038/35416

Takumi, T., K. Moriyoshi, I. Aramori, T. Ishii, S. Oiki, Y. Okada, H. Ohkubo, and S. Nakanishi. 1991. Alteration of channel activities and gating by mutations of slow I_{SK} potassium channel. *J. Biol. Chem.* 266:22192–22198.

Tapper, A.R., and A.L. George Jr. 2000. MinK subdomains that mediate modulation of and association with KvLQT1. *J. Gen. Physiol.* 116:379–390. doi:10.1085/jgp.116.3.379

Tapper, A.R., and A.L. George Jr. 2001. Location and orientation of minK within the I(Ks) potassium channel complex. *J. Biol. Chem.* 276:38249–38254.

Tyson, J., L. Tranebjaerg, M. McEntagart, L.A. Larsen, M. Christiansen, M.L. Whiteford, J. Bathen, B. Aslaksen, S.J. Sørland, O. Lund, et al. 2000. Mutational spectrum in the cardioauditory syndrome of Jervell and Lange-Nielsen. *Hum. Genet.* 107:499–503. doi:10.1007/s004390000402

Tzounopoulos, T., J. Maylie, and J.P. Adelman. 1998. Gating of I(sK) channels expressed in Xenopus oocytes. *Biophys. J.* 74:2299–2305. doi:10.1016/S0006-3495(98)77939-1

Vetter, D.E., J.R. Mann, P. Wangemann, J. Liu, K.J. McLaughlin, F. Lesage, D.C. Marcus, M. Lazdunski, S.F. Heinemann, and J. Barhanin. 1996. Inner ear defects induced by null mutation of the *isk* gene. *Neuron*. 17:1251–1264. doi:10.1016/S0896-6273(00)80255-X

Wang, K.W., and S.A. Goldstein. 1995. Subunit composition of minK potassium channels. *Neuron*. 14:1303–1309. doi:10.1016/0896-6273(95)90277-5

Wang, K.W., K.K. Tai, and S.A. Goldstein. 1996. MinK residues line a potassium channel pore. *Neuron*. 16:571–577. doi:10.1016/S0896-6273(00)80076-8

Xu, X., M. Jiang, K.L. Hsu, M. Zhang, and G.N. Tseng. 2008. KCNQ1 and KCNE1 in the IKs channel complex make state-dependent contacts in their extracellular domains. *J. Gen. Physiol.* 131:589–603. doi:10.1085/jgp.200809976